Nanosized complex fluorides based on Eu3+ doped Sr2LnF7 (Ln=La, Gd)

ARTICLE *in* JOURNAL OF RARE EARTHS · MARCH 2014

Impact Factor: 1.26 · DOI: 10.1016/S1002-0721(14)60058-2

3 AUTHORS, INCLUDING:

Marcin Runowski
Adam Mickiewicz University
22 PUBLICATIONS **132** CITATIONS
SEE PROFILE

Sangeetha Balabhadra
University of Aveiro
8 PUBLICATIONS **15** CITATIONS
SEE PROFILE

Available online at www.sciencedirect.com
ScienceDirect
JOURNAL OF RARE EARTHS, Vol. 32, No. 3, Mar. 2014, P. 242
JOURNAL OF RARE EARTHS
www.re-journal.com/en/

Nanosized complex fluorides based on Eu^{3+} doped Sr_2LnF_7 (Ln=La, Gd)

M. Runowski, S. Balabhadra, S. Lis*

(Department of Rare Earths, Faculty of Chemistry, Adam Mickiewicz University, Grunwaldzka 6, 60-780 Poznan, Poland)

Received 8 June 2013; revised 27 January 2014

Abstract: A simple co-precipitation approach taking place between Ln^{3+}, Sr^{2+} cations and F^- anions, led to the formation of nanocrystalline Eu^{3+} doped Sr_2LnF_7 (Ln=La and Gd) complex fluorides. The reaction was carried out in the presence of polyethylene glycol, PEG 6000 as a surfactant/surface modifier, providing small size and homogeneity of the products. The synthesized compounds were composed of small nanoparticles with an average size of 15 nm. All obtained Eu^{3+} doped compounds exhibited an intensive red luminescence. In the case of gadolinium based compounds, the energy transfer phenomena could be observed from Gd^{3+} ions to Eu^{3+} ions. In order to study the structure and morphology of the synthesized fluorides, powder X-ray diffraction (XRD) and transmission electron microscopy (TEM) measurements were performed. Also FT-IR spectra of the products were recorded, revealing the presence of PEG molecules on the nanoparticles surface. A spectrofluorometry technique was applied to examine optical properties of the synthesized nanoparticles. Excitation and emission spectra as well as luminescence decay curves were measured and analysed. The performed analysis revealed a red luminescence, typical for the Eu^{3+} ion situated in the inorganic, highly symmetric matrix. Concentration quenching phenomena and lifetimes shortening, together with an increasing of the Eu^{3+} doping level, were observed and discussed. Judd-Ofelt analysis was also performed for all doped samples, in order to support the registered spectroscopic data and examine in details structural and optoelectronic properties of the synthesized nanomaterials.

Keywords: luminescence; Eu^{3+} doping; complex strontium lanthanide fluorides; nanoparticles; Sr_2LnF_7; $Sr_{0.69}La_{0.31}F_{2.31}$; rare earths

Rare-earth-doped inorganic nanomaterials have been applied or considered for applications in modern lighting, displays and optical communication fields, such as fluorescent lamps, field emission displays, plasma display panels (PDPs)[1–5]. Recently, many researchers are paying much attention on lanthanide fluorides[6–8], alkaline earth metal fluorides[9,10] and complex ones[11–13]. Moreover, scientists successfully investigated Eu^{3+} doped alkaline earth fluorides as white light-emitting-diodes (WLEDs) materials[14].

The alkaline earth fluorides are important optical raw materials with high solubility of both sensitizer and activator ions, which have been applied as crystal laser hosts. Because the radii of the luminescent lanthanide ions are similar to the Sr^{2+} host cations, the Ln^{3+} ions can be successfully embedded in the Sr_2LnF_7 structure[14,15]. The concentration of the dopant ions also shows a predominant effect on their structural and optical characteristics in the strontium fluorides. Among all of the lanthanides, Eu^{3+} is most convenient for these kind of studies, due to narrow emission bands and long radiative lifetimes of the excited states. More importantly Eu^{3+} doping is regarded to be a luminescent probe that allows extraction of necessary information concerning a local chemical environment of lanthanide ion and crystal structure, directly from the emission spectra. Also an intensive red emission from the Eu^{3+} ion is a factor improving the color rendering index (CRI).

The fluoride hosts, such as the one studied in the current work, are strong and efficient luminescent materials. Nowadays, fluoride hosts, are intensively investigated due to their potential applications in many areas including lighting, optoelectronics, detection systems or more advanced forensic medical applications[16–18]. The lanthanide fluorides are especially interesting due to the low phonon energy of their crystal lattice, which suppresses nonradiative relaxations of dopant ions, like Eu^{3+} [19]. This value is significantly lower in comparison to lanthanide oxides, phosphates or borates, often used as phosphors. Due to their photostability, lanthanide fluorides can be used as special materials in novel applications[14].

In the this work we reported the luminescent nanomaterials containing Eu^{3+} doped Sr_2LnF_7:Eu^{3+} (Ln= La, Gd) nanocrystals. The structure, morphology and spectroscopic properties of the obtained products were examined, and the obtained results were analysed and discussed. The Judd-Ofelt theory was applied to calculate the radiative properties of the prepared materials, and to investigate their electron structure.

Foundation item: Project supported by Polish Ministry of Science and Higher Education (Diamond Grant" Nr DI2011 011441)

* **Corresponding author:** S. Lis (**E-mail:** blis@amu.edu.pl; **Tel.:** +48 61 829 1345)

DOI: 10.1016/S1002-0721(14)60058-2

1 Experimental

1.1 Synthesis

1.1.1 Materials

La_2O_3, Eu_2O_3 and Gd_2O_3 oxides (Stanford Materials, 99.99%) were separately dissolved in a concentrated, nitric acid, HNO_3 (POCh S.A., ultra-pure) to obtain $La(NO_3)_3$, $Eu(NO_3)_3$ and $Gd(NO_3)_3$ aqueous solutions, respectively. Strontium nitrate, $Sr(NO_3)_2$ (pure, 99%) and ammonium fluoride, NH_4F (ACS grade, ≥98%) were purchased from POCh S.A. Polyethylene glycol - PEG 6000 (Alfa Aesar, 98%) was used as a surfactants/surface modifier. In all experiments, only ultra-pure distilled water was used.

1.1.2 Synthesis

The synthesis of complex, nanocrystalline fluorides based on Eu^{3+} doped Sr_2LnF_7 (Ln=La and Gd) was performed via a simple wet chemical route, namely co-precipitation. To synthesize the Sr_2LnF_7:Eu^{3+} nanocrystals, the stoichiometric amounts of appropriate lanthanide salts were dissolved in 50 mL of ethanol/water solvent system. After that, 0.25 g of PEG 6000 was added and dissolved. Polyethylene glycol was used as a surfactant/surface modifier to provide small size and homogeneity for desired nanocrystals. Afterwards, second solution was prepared by dissolving NH_4F (50% excess) in 50 mL of the same water/ethanol system, with the addition of 0.25 g of PEG 6000, as well. Subsequently, the first solution was dropped into the solution containing fluoride ions, which was heated up to approx. 50 °C. The dropping process lasted approx. 20 min. Afterwards, the formed transparent precipitate was collected and washed with water for several times. The final obtained product was dried in vacuum at 85 °C for 12 h.

1.2 Characterization

Electron microscopy measurements were performed using a transmission electron microscope JEM 1200 EXII, JEOL, operating at accelerating voltage equal to 80 kV. Powder X-ray diffractograms were registered using Bruker AXS D8 Advance diffractometer, using Cu Kα radiation (λ=0.15406 nm). Based on the experimental XRD patterns, the average grains sizes were estimated using Scherrer's equation:

$$D = \frac{k\lambda}{\cos\theta\sqrt{\beta - \beta'^2}} \quad (1)$$

Where D is grain size, k is a shape factor (0.9 for spherical particles), λ is a wavelength of radiation, θ is an angle of diffraction, β is a full width at half maximum (FWHM) and β'^2 is an instrumental effect. IR spectra were measured with FT-IR spectrophotometer, JASCO 4200. The IR spectra were measured in transmission mode; the samples were mixed with KBr, ground and pressed into pellets. The excitation, emission spectra and luminescence decay curves were registered using Hitachi F-7000 spectrofluorometer at ambient conditions. The excitation and emission spectra were appropriately corrected for the apparatus response.

2 Results and discussion

The structures of the synthesized products were studied using powder XRD technique. Both series of the obtained Eu^{3+} doped fluorides crystallize as cubic, complex fluoride $Sr_xLn_{1-x}F_y$ (Ln=La, Gd) isostructural with SrF_2[14]. Because of the similarity of the ionic radii of Sr^{2+} and Ln^{3+}, both Ln^{3+} ions can easily substitute the Sr^{2+} ions in the crystal lattice, forming the above mentioned complex fluorides[15]. The occurring phenomenon was also confirmed as a presence of one, crystalline phase in the presented powder diffractograms (Fig. 1) of the synthesized nanomaterials, in the whole doping range (0–30% Eu^{3+}). All diffractograms were compared and fitted well to the $Sr_{0.69}La_{0.31}F_{2.31}$ (ICDD card No. 04-006-8267), crystallising in a cubic crystal system, *Fm*3*m* space group. The Sr/Ln ratio is close to 2 in the discussed structure, like the molar ratios of Sr^{2+} and Ln^{3+} ions used as starting materials in the synthesis process. For the convenience of the reader the empiric formula Sr_2LnF_7:Eu^{3+} *x*% (equal to $Sr_2Ln_{1-x}Eu_xF_7$) was used throughout this article. The synthesized doped Sr_2GdF_7 reveal shifted XRD patterns towards higher 2θ angles, compared to the analogic Sr_2LaF_7 compounds, which means that their unit cell parameters decreased. The mentioned phenomenon is in good agreement with the well-known lanthanide contraction, due to the fact that the Gd^{3+} ion has smaller ionic radius than the La^{3+} ion. Because of the same reasons, increasing amount of the Eu^{3+} ions in the Sr_2LaF_7:Eu^{3+} series (ranging from 0 to 30%), the same shift towards higher angles can be observed. In the case of Sr_2GdF_7:Eu^{3+} series, a slight shift, however towards smaller angle can be observed, as well (unit cell volume expansion, due the slightly larger Eu^{3+} ionic radius in comparison with substituted Gd^{3+} ion). All measured XRD patterns of the synthesized nanomaterials reveal significant broadening effect of their reflexes, which is characteristic for nanocrystalline products, and confirms their small, nanometric size. Based on Scherrer equation[20], the average grain size for the obtained Eu^{3+} doped Sr_2LaF_7 and Sr_2GdF_7 series were estimated as 8.26±0.76 nm and 8.76±0.94 nm, respectively (because of the same reflexes broadening in each series, the estimated grain sizes are averaged values for each Eu^{3+} doped series). The obtained grain size values correspond well to the data calculated from TEM images. However, they are a bit smaller, probably because of the presence of strains/defects in the crystal structure of the synthesized nanomaterials, which is common in such small nanoparticles and causes reflexes broadening, as well.

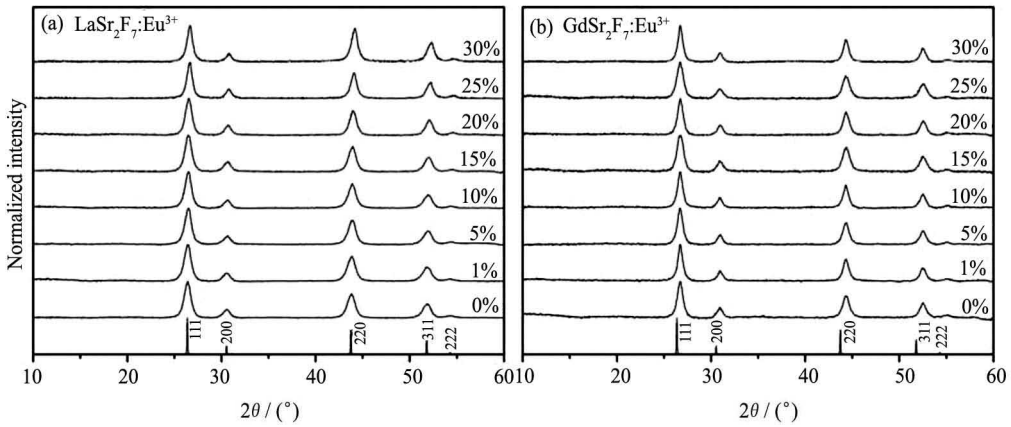

Fig. 1 XRD patterns of Eu^{3+} doped Sr_2LaF_7 (a) and Sr_2GdF_7 (b)

The complementary information about the structure and morphology of the obtained nanomaterials are provided using transmission electron microscopy (TEM) technique. Fig. 2 depicts TEM images of Sr_2LaF_7: 20%Eu^{3+} (a) and Sr_2GdF_7:20%Eu^{3+} (b) nanocrystals. By using PEG 6000 as a surfactant, the obtained nanomaterials are composed of relatively uniform, small and homogeneous nanocrystals, which is clearly seen in the depicted pictures. The synthesized nanoparticles of both products are in the range of 10–15 nm. The morphology of the obtained nanostructures is also similar in each series with the varying Eu^{3+} level (data not shown), however La^{3+} based fluorides are generally less agglomerated than Gd^{3+} based ones.

In the depicted FT-IR spectra (Fig. 3) of the Sr_2LaF_7: 20%Eu^{3+} and Sr_2GdF_7:20%Eu^{3+} products, the presence of the organic compound (PEG 6000 – surface modifier) attached to the nanoparticles surface can be observed. This fact is confirmed by the presence of absorption peaks, originating from organic moieties oscillations of polyethylene glycol molecules. Peaks at 2933 and 2884 cm^{-1} are related with stretching vibrations of C–H bonds in $–CH_2$ groups, and the peak at 1436 cm^{-1} corresponds to the bending vibrations of these groups. The strong and sharp peak at 1384 cm^{-1} originates from bending vibrations within –OH groups of polyethylene glycol. The rest of the peaks are related to absorbed, surface water molecules (νO–H at 3400 cm^{-1} and σO–H at 1640 cm^{-1}) and CO_2 molecules (approx. 2360 cm^{-1}).

Here we presented luminescence properties of the obtained nanomaterials, expressed as a comparison of their excitation and emission spectra, luminescence decay curves and Judd-Ofelt analysis.

The measured excitation spectra presented in Fig. 4, were registered at λ_{em}=593 nm (the range of the most prominent band corresponding to the $^5D_0 \rightarrow {}^7F_1$ transition), in the range of 200–450 nm, and normalized to the intensity of the most intensive band in each spectrum. The first series of excitation spectra for Sr_2LaF_7 (Fig. 4) exhibit numerous sharp, characteristic bands, related with intrinsic $4f^8$-$4f^8$ transitions within Eu^{3+} ions, visible mainly in the 240–400 nm range. All transitions reveal similar intensities in the whole range of the applied doping. The second set of the excitation spectra registered for Sr_2GdF_7 (Fig. 4), besides the same bands typical for transitions in Eu^{3+} ions, reveals two additional bands related with $^8S_{7/2} \rightarrow {}^6I_J$ (*ca.* 272 nm) and $^8S_{7/2} \rightarrow {}^6P_J$ (*ca.* 310 nm) transitions of the Gd^{3+} ions, corresponding to $Gd^{3+} \rightarrow Eu^{3+}$ energy transfer (ET)[7]. The high intensity of those bands is caused by an effective overlapping of the donor (Gd^{3+}) emission and acceptor (Eu^{3+}) absorption integral. Because of this phenomenon the ET process is very efficient in the obtained nanomaterials. Together with the increment of the amount of dopant ions (Eu^{3+}),

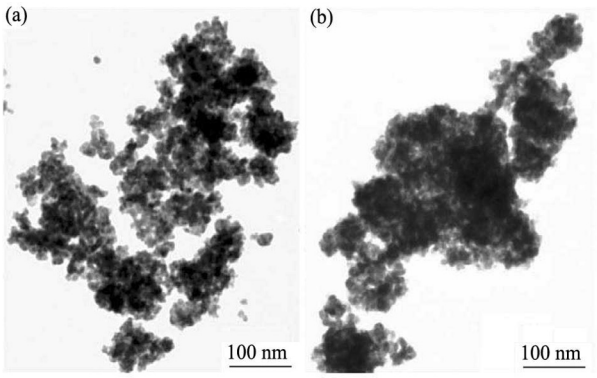

Fig. 2 TEM images of $Sr_2LaF_7:Eu^{3+}$ 20% (a) and $Sr_2GdF_7:Eu^{3+}$ 20% (b)

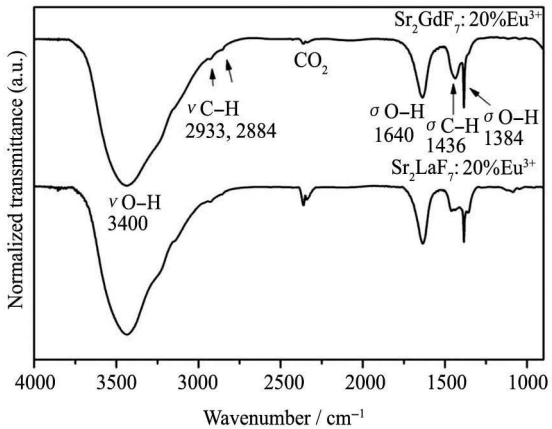

Fig. 3 FT-IR spectra of Sr_2LaF_7:20%Eu^{3+} and Sr_2GdF_7:20%Eu^{3+}

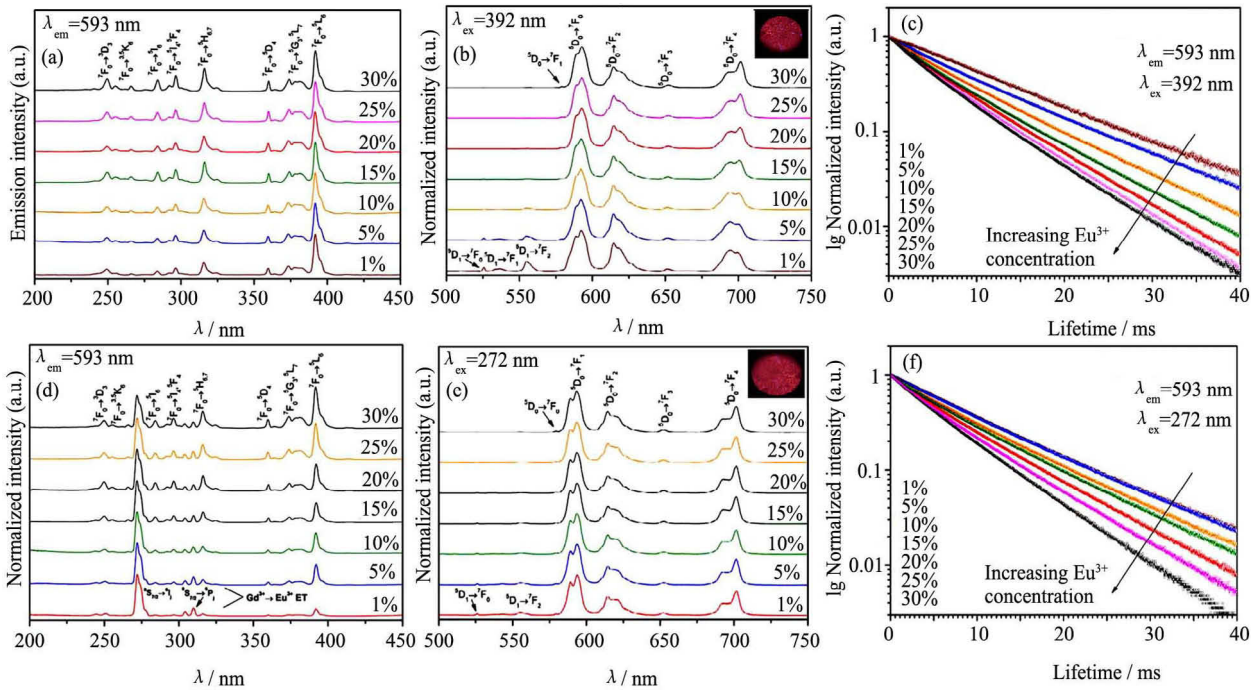

Fig. 4 Excitation (a, d), emission (b, e) spectra and luminescence decay curves (c, f) of Eu^{3+} doped Sr_2LaF_7 (a–c) and Sr_2GdF_7 (d–f)

the most prominent band, namely $^8S_{7/2}\rightarrow{}^6I_J$ related with $Gd^{3+}\rightarrow Eu^{3+}$ ET, becomes less intensive in comparison to the rest bands originating from intrinsic transitions in the Eu^{3+} ions, which can be observed in the discussed spectra. In the case of the $Sr_2Gd_{0.7}Eu_{0.3}F_7$ sample with the highest doping level, the $^7F_0\rightarrow{}^5L_6$ band (related with intrinsic transitions in Eu^{3+} ion) is even more intense than the $^8S_{7/2}\rightarrow{}^6I_J$ band. The discussed altering of the mentioned transitions ratio is directly related with decreasing amount of Gd^{3+} ions in the samples together with an increase of Eu^{3+} doping.

Emission of the observed bands is generally similar in all synthesized products. In both, La and Gd based compounds the emission from higher energy excited levels is the most efficient in the samples with lower doping levels (1% and 5% of Eu^{3+}), because when the concentration of Eu^{3+} ions increases in the sample, the mentioned higher excited levels are effectively quenched, which is a well-known phenomenon in the case of Eu^{3+} doped materials[21]. The hypersensitive $^5D_0\rightarrow{}^7F_2$ electric dipole transition (forbidden transition, the intensity increases when the site symmetry of Eu^{3+} ion decreases[22]) in all spectra is relatively weak, in comparison with $^5D_0\rightarrow{}^7F_1$ magnetic dipole transition, which acts usually as an internal standard in the case of transitions ratio comparisons in Eu^{3+} doped compounds. The mentioned fact clearly states that a local symmetry of the environment of the Eu^{3+} ions in the obtained nanomaterials is relatively high. This is in a good agreement with our predictions, and states that the Eu^{3+} dopant ions were successfully incorporated in the ordered, highly crystalline, cubic structure of the synthesized fluorides, where the site symmetry is high.

Luminescence lifetimes were analysed based on registered luminescence decay curves of the obtained nanophosphors, and are shown in Fig. 4. All curve profiles were fitted well (R>0.999) to the mathematic function $y=A_1*\exp(-x/\tau)+y_0$, demonstrating the monoexponential character of the measured luminescence decay curves. This was in good accordance with our prediction, due to the presence of only one coordination site which can be occupied by Ln^{3+} ions, in the synthesized fluoride crystal structures. In both series of obtained compounds, the general trend expressed by the lifetimes shortening together with an increment of doping level (more Eu^{3+} ions in the crystal structure) can be observed. All calculated lifetimes are relatively long and are in the range of ms (3.9–7.6 ms), which is typical for crystalline Eu^{3+} doped fluorides[7]. The exact values of lifetimes for all obtained compounds were calculated as averaged luminescence lifetimes, namely $\tau=\int I(\tau)\tau dt/\int I(\tau)dt$, and are presented in Table 1, together with data obtained from Judd-Ofelt analysis.

Based on the measured luminescence properties of the synthesized nanophosphors, the comparison of their integral luminescence intensity was plotted and is presented in Fig. 5. In both examples, Sr_2LaF_7:Eu^{3+} (λ_{ex}=392 nm) and Sr_2GdF_7:Eu^{3+} (λ_{ex}=272 nm), the most intensive luminescence exhibited compounds doped with 20% of Eu^{3+} ($Sr_2La_{0.8}Eu_{0.2}F_7$). This observation is in good agreement with cross relaxation model, which is at the higher doping level (using luminescence activator ion as a dopant e.g. Eu^{3+}), the concentration quenching phenomenon occurs[21]. In the case of our nanophosphors

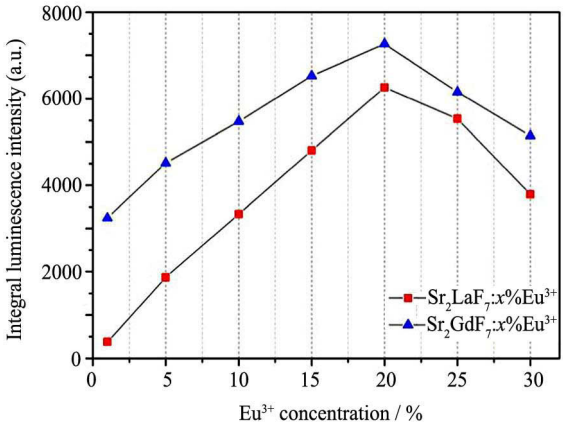

Fig. 5 Integral luminescence intensity for Eu^{3+} doped Sr_2LaF_7 and Sr_2GdF_7

that critical doping level was achieved when more than 20% of the Ln^{3+} ions were substituted by Eu^{3+} ions. The gadolinium based products exhibit generally more intensive luminescence than lanthanum based ones, which can be observed in the depicted plot.

The analysis of Judd-Ofelt intensity parameters was performed in order to support and extend the registered spectroscopic data, as well as to provide more detailed information concerning the structural and photophysical aspects of the obtained nanomaterials. The mentioned analysis has been carried out based on the well-known procedure described by Kodaira et al.[23] and successfully applied by others[7,24]. The refractive index for all compounds was assumed to be 1.44, as for isostructural SrF_2. In general, the Ω_2 intensity parameter is related to the local site symmetry of the Eu^{3+} ion, and its polarizability. The value of this parameter increases with increasing asymmetry of the coordination environment of the Eu^{3+} ions present in the crystalline host. The Ω_4 intensity parameter is related to the bond covalency in the system (electron density within the ligands) and its rigidity. Higher value of this parameter corresponds to higher covalency (lesser iconicity) of the system. In both series of products the values of the Ω_2 parameters are similar because of the same cubic crystal structure of all doped compounds, in which the symmetry is generally similar. However, in the Sr_2LaF_7:Eu^{3+} series a slight decrease of the Ω_2 value with increasing Eu^{3+} concentration was observed (decreasing $^5D_0 \rightarrow {}^7F_2/{}^5D_0 \rightarrow {}^7F_1$ transitions ratio in the emission spectra). The Ω_4 value increases in the Sr_2LaF_7:Eu^{3+} series with the increase of Eu^{3+} doping. This phenomenon is related with increasing covalency of the Ln–F bond. Due to the well-known lanthanide contraction[25], Eu^{3+} has smaller ionic radius than La^{3+}, that is why the average distance between Ln^{3+} and F^- decreases, resulting in increased bond covalency in this system. There are no clear tendencies of the $\Omega_{2,4}$ parameters in the Sr_2GdF_7:Eu^{3+} series, because of the similar ionic radii of Eu^{3+} and Gd^{3+} ions[26]. In the case of the calculated quantum yield of luminescence, also the decreasing tendency (from approx. 98% to 50%) in both series is visible. Therefore an increasing Eu^{3+} concentration in the samples causes decreasing of quantum yield, because of the stronger cross-relaxation process between Eu^{3+} ions in the compounds of higher doping level.

Table 1 Radiative (A_{rad}) and non-radiative (A_{nrad}) decay rates, total processes of $^5D_0 \rightarrow {}^7F_J$ transitions (A_{tot}), luminescence lifetimes (τ), intensity parameters (Ω_2 and Ω_4) and quantum yield of luminescence (η) for Eu^{3+} doped Sr_2GdF_7 (top) and Sr_2LaF_7 (bottom)

Sr_2GdF_7: x%Eu^{3+}	A_{rad}/ s^{-1}	A_{nrad}/ s^{-1}	A_{tot}/ s^{-1}	τ/ ms	Ω_2/ 10^{-20} cm^2	Ω_4/ 10^{-20} cm^2	η/ %
1	126.13	26.54	152.67	6.55	5.44	12.34	82.61
5	125.78	27.12	152.91	6.54	5.28	12.30	82.26
10	125.45	50.29	175.75	5.69	5.41	12.68	71.38
15	124.75	69.42	194.17	5.15	4.88	12.85	64.25
20	127.92	86.68	214.59	4.66	5.31	12.73	59.61
25	126.98	111.10	238.09	4.20	5.28	12.73	53.34
30	128.92	128.15	257.07	3.89	5.59	12.66	50.15
Sr_2LaF_7: x%Eu^{3+}	A_{rad}/ s^{-1}	A_{nrad}/ s^{-1}	A_{tot}/ s^{-1}	τ/ ms	Ω_2/ 10^{-20} cm^2	Ω_4/ 10^{-20} cm^2	η/ %
1	130.180	2.09	132.27	7.56	5.85	12.22	98.41
5	130.63	26.35	156.98	6.37	6.07	12.21	83.21
10	129.84	56.72	186.56	5.36	5.96	12.23	69.59
15	129.42	80.22	209.64	4.77	5.75	12.54	61.73
20	129.15	95.56	224.71	4.45	5.67	12.58	57.47
25	131.58	105.38	236.96	4.22	5.64	13.11	55.52
30	133.64	119.52	253.16	3.95	5.63	14.05	52.78

3 Conclusions

The synthesis of complex, nanocrystalline fluorides based on Eu^{3+} doped Sr_2LnF_7 (Ln=La and Gd) was successfully performed via a simple and low-cost co-precipitation route. The synthesized products were composed of small (approx. 15 nm) nanoparticles. Polyethylene glycol was used as a surfactant/surface modifier, providing small size and homogeneity of the obtained nanocrystals, and its presence was confirmed by FT-IR spectroscopy. The structure and morphology of the synthesized nanomaterials were examined and confirmed by transmission electron microscopy (TEM) and powder X-ray diffraction (XRD) techniques. Spectroscopic studies (excitation, emission spectra and luminescence decay curves measurements) for all synthesized samples were supported by detailed Judd-Ofelt analysis, revealing structural and local site symmetry changes after Ln^{3+} substitution in the crystal structure. The obtained compounds could be potentially used as efficient nanophosphors due to their bright and intensive red luminescence under UV irradiation, as well as for the sophisticated, hybrid core/shell type nanostructures functioning as small and luminescent nanocrystalline core.

References:

[1] Hölsä J. Persistent luminescence beats the afterglow: 400 years of persistent luminescence. *Electrochem. Soc. Interface*, 2009, winter: 42.

[2] Chander H. Development of nanophosphors - A review. *Mater. Sci. Eng*., 2005, **49**: 113.

[3] Shionoya S, Yen W M. Phosphor Handbook. Boca Raton, Florida: CRC Press, 1999.

[4] Kim C. Phosphors for plasma display panels. *J. Alloys Compd*., 2000, **311**: 33.

[5] Shyichuk A, Lis S. Green-emitting nanoscaled borate phosphors $Sr_3RE_2(BO_3)_4:Tb^{3+}$. *Mater. Chem. Phys.*, 2013, **40**: 447.

[6] Grzyb T, Runowski M, Szczeszak A, Lis S. Influence of matrix on the luminescent and structural properties of glycerine-capped, Tb^{3+} doped fluoride nanocrystals. *J. Phys. Chem. C*, 2012, **116**: 17188.

[7] Grzyb T, Runowski M, Szczeszak A, Lis S. Structural, morphological and spectroscopic properties of Eu^{3+} doped rare earth fluorides synthesized by the hydrothermal-method. *J. Solid State Chem*., 2013, **200**: 76.

[8] Li C X, Ma P A, Yang P P, Xu Z H, Li G G, Yang D M, Peng C, Lin J. Fine structural and morphological control of rare earth fluorides REF_3 (RE=La–Lu, Y) nano/microcrystals: microwave-assisted ionic liquid synthesis, magnetic and luminescent properties. *CrystEngComm*, 2011, **13**: 1003.

[9] Moore D S. Laser spectroscopy of defect chemistry in $CaF_2:Er^{3+}$, *J. Chem. Phys*., 1981, **74**: 1626.

[10] Wang J S, Miao W R, Li Y X, Yao H C, Li Z J. Water-soluble Ln^{3+}- doped calcium fluoride nanocrystals: Controlled synthesis and luminescence properties. *Mater. Lett.*, 2009, **63**: 1794.

[11] Marcazzó J, Santiago M, D'Angelo C, Furetta C, Caselli E, Study of the luminescent properties of $KMgF_3$:Sm. *Nucl. Instrum. Methods Phys. Res*., *Sect. B*, 2010, **268**: 183.

[12] Wang F, Fan X P, Wang M Q, Zhang Y. Multicolour PEI/$NaGdF_4:Ce^{3+}$, Ln^{3+} nanocrystals by single-wavelength excitation. *Nanotechnology*, 2007, **8**: 25701.

[13] Wang L L, Chen H, Zhang D S, Zhao D, Qin W P. Dual-mode luminescence from lanthanide tri-doped $NaYF_4$ nanocrystals. *Mater. Lett*., 2011, **65**: 504.

[14] Fu H Y, Qiao X S, Cui S, Luo Q, Qian J Y, Fan X P, Zhang X H. Tunable white light emission from glass-ceramics containing Eu^{2+}, Tb^{3+}, Eu^{3+} co-doped $SrLaF_5$ nanocrystals. *Mater. Lett.*, 2012, **71**: 15.

[15] Qiao X S, Fan X P, Wang M Q, Yang H, Zhang X F. Luminescence behavior of Er^{3+} doped glass ceramics containing Sr_2RF_7 (R=Y, Gd, La) nanocrystals. *J. Appl. Phys*., 2008, **104**: 43508.

[16] Wegh R.T. Visible quantum cutting in $LiGdF_4:Eu^{3+}$ through downconversion. *Science*, 1999, **283**: 663.

[17] Cui S S, Chen H Y, Zhu H Y, Tian J M, Chi X M, Qian Z Y, Achilefu S, Gu Y Q. Amphiphilic chitosan modified upconversion nanoparticles for in vivo photodynamic therapy induced by near-infrared light. *J. Mater. Chem.*, 2012, **22**: 4861.

[18] Singh K, Kumar K, Pandey C, Parkash O, Rai S B, Kumar D. Photon avalanche upconversion and pump power studies in $LaF_3:Er^{3+}/Yb^{3+}$ phosphor. *Appl. Phys. B*, 2011, **104**: 1035.

[19] Wang J S, Bo S H, Song L M, Hu J, Liu X H, Zhen Z. One-step synthesis of highly water-soluble $LaF_3:Ln^{3+}$ nanocrystals in methanol without using any ligands. *Nanotechnology*, 2007, **18**: 465606.

[20] Langford J I, Wilson J C. Scherrer after sixty years: A survey and some new results in the determination of crystallite size. *J. Appl. Crystallogr.*, 1978, **11**: 102.

[21] Blasse G. Concentration quenching of Eu^{3+} fluorescence. *J. Chem. Phys*., 1967, **46**: 2583.

[22] Judd B R. Hypersensitive transitions in rare-earth ions. *J. Chem. Phys*. 1966, **44**: 839.

[23] Kodaira C, Brito H F, Malta O L, Serra O A. Luminescence and energy transfer of the europium (III) tungstate obtained via the Pechini method. *J. Lumin*., 2003, **101**: 11.

[24] Wiglusz R J, Grzyb T, Lis S, Strek W. Hydrothermal preparation and photoluminescent properties of $MgAl_2O_4:Eu^{3+}$ spinel nanocrystals. *J. Lumin*., 2010, **130**: 434.

[25] Runowski M, Grzyb T, Lis S. Bifunctional luminescent and magnetic core/shell type nanostructures Fe_3O_4@CeF_3:Tb^{3+}/SiO_2. *J. Rare Earths*, 2011, **29**: 1117.

[26] Runowski M, Grzyb T, Lis S. Magnetic and luminescent hybrid nanomaterial based on Fe_3O_4 nanocrystals and $GdPO_4:Eu^{3+}$ nanoneedles. *J. Nanopart. Res*., 2012, **14**: 1188.